Boundary layer flow and heat transfer to Carreau fluid over a nonlinear stretching sheet

Masood Khan and ⓘD Hashim

ARTICLES YOU MAY BE INTERESTED IN

Analysis of the Casson and Carreau-Yasuda non-Newtonian blood models in steady and oscillatory flows using the lattice Boltzmann method
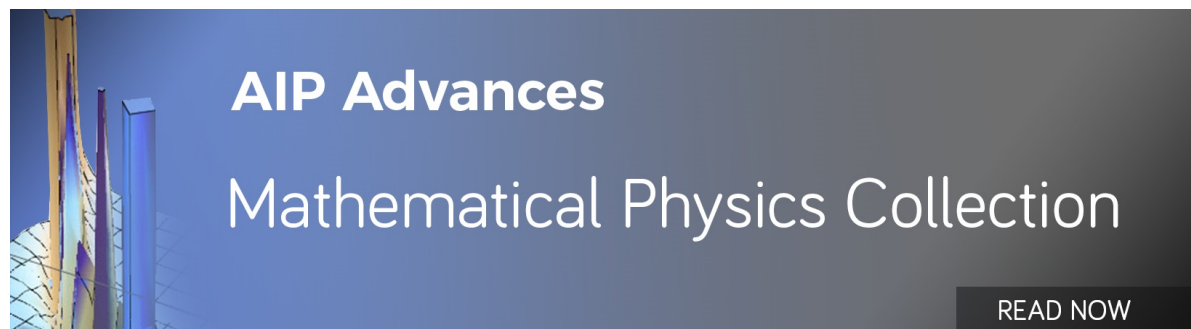Physics of Fluids **19**, 093103 (2007); https://doi.org/10.1063/1.2772250

Rheological Equations from Molecular Network Theories
Transactions of the Society of Rheology **16**, 99 (1972); https://doi.org/10.1122/1.549276

Impact of Cattaneo-Christov heat flux in the flow over a stretching sheet with variable thickness
AIP Advances **5**, 087159 (2015); https://doi.org/10.1063/1.4929523

AIP Advances

Mathematical Physics Collection

READ NOW

Boundary layer flow and heat transfer to Carreau fluid over a nonlinear stretching sheet

Masood Khan and Hashim[a]

Department of Mathematics, Quaid-i-Azam University, Islamabad 44000, Pakistan

This article studies the Carreau viscosity model (which is a generalized Newtonian model) and then use it to obtain a formulation for the boundary layer equations of the Carreau fluid. The boundary layer flow and heat transfer to a Carreau model over a nonlinear stretching surface is discussed. The Carreau model, adequate for many non-Newtonian fluids, is used to characterize the behavior of the fluids having shear thinning properties and fluids with shear thickening properties for numerical values of the power law exponent n. The modeled boundary layer conservation equations are converted to non-linear coupled ordinary differential equations by a suitable transformation. Numerical solution of the resulting equations are obtained by using the Runge-Kutta Fehlberg method along with shooting technique. This analysis reveals many important physical aspects of flow and heat transfer. Computations are performed for different values of the stretching parameter (m), the Weissenberg number (We) and the Prandtl number (Pr). The obtained results show that for shear thinning fluid the fluid velocity is depressed by the Weissenberg number while opposite behavior for the shear thickening fluid is observed. A comparison with previously published data in limiting cases is performed and they are in excellent agreement. © *2015 Author(s). All article content, except where otherwise noted, is licensed under a Creative Commons Attribution 3.0 Unported License.* [http://dx.doi.org/10.1063/1.4932627]

I. INTRODUCTION

For the chemical engineering industry the most important property of fluids is the non-Newtonian viscosity. The generalized Newtonian fluids are those in which the viscosity changes with the shear rate i.e. the viscosity of the fluid shows a dependence on the shear rate. The change in the viscosity by two or three orders of magnitude is feasible for some fluids and this cannot be ignored when the lubrication problems and polymer processing is considered. Therefore, one of the basic empirically obtained modifications of the Newton's law of viscosity is to allow the viscosity to change with the shear rate. Such variety of fluids is commonly referred to as generalized Newtonian fluids and explained in Bird *et al.*[1] The simplest generalized Newtonian fluid is the power-law constitutive relation. The power-law viscosity model has the limitation that it cannot adequately predict the viscosity for very small or very large shear rates. In view of such limitation of the power law model, especially for very low and very high shear rates, we consider another viscosity model from the class of generalized Newtonian fluids, namely Carreau rheological model.[2] This model overcomes the limitations of the power-law model identified above and appears to be gaining wider acceptance in chemical engineering and technological processes. The Carreau fluid model can well characterize the rheology of various polymeric solutions, such as 1% methylcellulose tylose in glycerol solution and 0.3% hydroxyethyl-cellulose Natrosol HHX in glycerol solution[3] and pure poly ethylene oxide.[4] These polymers are widely used in capillary electrophoresis to improve the resolution in the separation of proteins[5] and DNAs.[6] It determines a specific region where the fluid viscosity and its shear rate has a linear relationship (on the usual log-log coordinates). Thus, the

[a]Corresponding author: Electronic mail: hashim_alik@yahoo.com (Hashim).

Carreau model predicts a power law region. However, unlike the power-law model, it anticipate a viscosity which remains finite as the shear rate approaches zero. Due to this reason, the constitutive equation of the Carreau model is much suitable for free surface flows.

Due to wider applications, the Carreau model has caught the attention of many researchers and engineers during the last few years. Chhabra and Uhlherr[7] and Bush and Phan-Thein[8] studied the flows of the Carreau fluid model around the spheres. Later on, Hsu and Yeh[9] investigated the drag on two coaxial rigid spheres which moving along the axis of a cylinder filled with Carreau fluid. Uddin et al.[10] discussed the squeeze flow of a Carreau fluid during sphere impact. Shadid and Eckert[11] presented the flow of a Carreau fluid over a cylinder. Tshehla[12] discussed the motion of a Carreau fluid along an inclined plane with a free surface. Olajuwon[13] investigated the MHD flow of Carreau fluid with convective heat and mass transfer over a vertical porous plat. Griffiths[14] discussed the flow of a generalized Newtonian fluid due to a rotating disk. He investigated that the base flow similarity solution is still applicable when we consider the Carreau model instead of power-law model.

The problem of boundary layer flow behavior because of a stretching sheet got the attention of many researchers as it has important bearing on many technological processes. Specifically, flow due to stretching surface is usually encountered in extrusion process where a melt is stretched into a cooling liquid. Other examples includes glass-fiber, cooling of continuous stripes and crystal growing. For these cases, the fluid product of our desired properties strictly depend on the stretching rate and the rate of cooling in the process. mechanical properties of the fluid desired for the outcome of such a process would mostly depend on the cooling rate and the rate of stretching. Initially, Sakiadis[15] study the boundary layer flow behavior for the solid surface which moves with constant speed. After that, many researchers studied the different aspect of these flows. Crane[16] and Gupta and Gupta[17] have studied the heat and mass transfer over a stretching sheet with constant surface temperature. Numerical solutions of Magnetohydrodynamic boundary layer flow of tangent hyperbolic fluid flow towards a stretching sheet with magnetic field is discussed by N. S. Akbar.[18] Nadeem et al.[19] investigated the MHD flow of a Casson fluid over an exponentially shrinking sheet. The boundary layer flow on an inextensible continuous flat sheet having constant velocity in a non-Newtonian power-law fluid is examine by Erickson et al.[20] using both exact and numerical schemes. Akbar et al.[21] discussed the dual solutions in MHD stagnation-point flow of Prandtl fluid impinging on shrinking sheet. The classical problem of two-dimensional flow induced by a non-linearly stretching sheet was described by Vajravelu.[22] Cortell[23] modified the problem by taking viscous dissipation effect and variable surface temperature. MHD three-dimensional Casson fluid flow past a porous linearly stretching sheet is examined by Nadeem et al.[24]

The objective of present investigation is to discuss the boundary layer flow and heat transfer of Carreau model over a non-linear stretching surface. We obtained the boundary layer equations for the velocity field of the Carreau fluid. This model which, in comparison with the Newtonian case involves three additional dimensionless parameters, allows the characterization of a wide variety of shear-thinning fluids. The numerical method namely Runge-Kutta shooting method is used to solve the nonlinear governing problem. The obtained results for both the fluid velocity and its temperature are presented for different values of parameters entering in the problem. The effects of emerging parameters, like the Weissenberg number We, the power law index n and the Prandtl number Pr on the local skin friction and local Nusselt number are presented numerically in tabular form.

II. GOVERNING EQUATIONS

The fundamental equations for the flow of an incompressible fluid are the conservation of mass, linear momentum and energy. We express these equations in the absence of body forces as follows:

$$\text{div } \mathbf{V} = 0, \tag{1}$$

$$\rho \frac{d\mathbf{V}}{dt} = \text{div } \boldsymbol{\tau}, \tag{2}$$

$$\rho c_p \frac{dT}{dt} = \boldsymbol{\tau}.\mathbf{L} - \text{div } \mathbf{q}, \tag{3}$$

where $\mathbf{V}$ represents the velocity field, ρ is the density of the fluid, $\boldsymbol{\tau}$ the Cauchy stress tensor, T the fluid temperature, c_p the specific heat, $\mathbf{q} = -k \, \mathrm{grad}\, T$, the heat flux with k the thermal conductivity of fluid, $\mathbf{L} = \nabla \mathbf{V}$ and d/dt denotes the total time derivative.

The Cauchy stress tensor for the Carreau rheological model is given by the following equation[1]

$$\boldsymbol{\tau} = -p\mathbf{I} + \eta \mathbf{A}_1, \tag{4}$$

with

$$\eta = \eta_\infty + (\eta_0 - \eta_\infty) \left[1 + (\Gamma\dot{\gamma})^2 \right]^{\frac{n-1}{2}}, \tag{5}$$

in which p denotes the pressure, $\mathbf{I}$ represents the identity tensor, η_0 is the zero-shear-rate viscosity, η_∞ the infinite-shear-rate viscosity, Γ a material time constant, and n expresses the power law index (since it describes the slope of $(\eta - \eta_\infty)/(\eta_0 - \eta_\infty)$ in the power law region). The shear rate $\dot{\gamma}$ is expressed as

$$\dot{\gamma} = \sqrt{\frac{1}{2} \sum_j \sum_j \dot{\gamma}_{ij} \dot{\gamma}_{ji}} = \sqrt{\frac{1}{2}\Pi} = \sqrt{\frac{1}{2} tr\left(\mathbf{A}_1^2\right)}. \tag{6}$$

Here Π is the second invariant strain rate tensor and

$$\mathbf{A}_1 = (\mathrm{grad}\,\mathbf{V}) + (\mathrm{grad}\,\mathbf{V})^{\mathrm{T}}. \tag{7}$$

We consider the most practical cases where in $\eta_0 >> \eta_\infty$.[25] Hence, η_∞ is taken to be zero and consequently Eq. (4) reduces as

$$\boldsymbol{\tau} = -p\mathbf{I} + \eta_0 \left[1 + (\Gamma\dot{\gamma})^2 \right]^{\frac{n-1}{2}} \mathbf{A}_1, \tag{8}$$

The Carreau-model with fluid index in the range $0 < n < 1$ are commonly referred as shear thinning or pseudoplastic fluids and Carreau fluids with fluid index in the range $n > 1$ are commonly referred as shear thickening or dilatant fluids.

For an incompressible two-dimensional flow, the velocity and temperature fields are assumed as

$$\mathbf{V} = [u(x, y), v(x, y), 0], \quad T = T(x, y), \tag{9}$$

where u and v represents the components of velocity vector along the $x-$ and $y-$ axis.

Making use of Eqs. (7) and (9) into Eq. (6), the rate of strain $\dot{\gamma}$ is expressed as:

$$\dot{\gamma} = \left[4\left(\frac{\partial u}{\partial x}\right)^2 + \left(\frac{\partial u}{\partial y} + \frac{\partial v}{\partial x}\right)^2 \right]^{1/2}. \tag{10}$$

Using Eq. (9) into Eqs. (1) and (2), keeping in view Eqs. (7), (8) and (10), a straightforward calculations gives the equations for conservation of mass and linear momentum as follows:

$$\frac{\partial u}{\partial x} + \frac{\partial v}{\partial y} = 0, \tag{11}$$

$$\rho\left(u\frac{\partial u}{\partial x} + v\frac{\partial u}{\partial y}\right) = -\frac{\partial p}{\partial x} + \eta_0\left(\frac{\partial^2 u}{\partial x^2} + \frac{\partial^2 u}{\partial y^2}\right)\left[1 + \Gamma^2\left\{4\left(\frac{\partial u}{\partial x}\right)^2 + \left(\frac{\partial u}{\partial y} + \frac{\partial v}{\partial x}\right)^2\right\}\right]^{\frac{n-1}{2}}$$
$$+ 2\eta_0\frac{\partial u}{\partial x}\frac{\partial}{\partial x}\left[1 + \Gamma^2\left\{4\left(\frac{\partial u}{\partial x}\right)^2 + \left(\frac{\partial u}{\partial y} + \frac{\partial v}{\partial x}\right)^2\right\}\right]^{\frac{n-1}{2}}$$
$$+ \eta_0\left(\frac{\partial u}{\partial y} + \frac{\partial v}{\partial x}\right)\frac{\partial}{\partial y}\left[1 + \Gamma^2\left\{4\left(\frac{\partial u}{\partial x}\right)^2 + \left(\frac{\partial u}{\partial y} + \frac{\partial v}{\partial x}\right)^2\right\}\right]^{\frac{n-1}{2}}, \tag{12}$$

$$\rho\left(u\frac{\partial v}{\partial x} + v\frac{\partial v}{\partial y}\right) = -\frac{\partial p}{\partial y} + \eta_0\left(\frac{\partial^2 v}{\partial x^2} + \frac{\partial^2 v}{\partial y^2}\right)\left[1 + \Gamma^2\left\{4\left(\frac{\partial u}{\partial x}\right)^2 + \left(\frac{\partial u}{\partial y} + \frac{\partial v}{\partial x}\right)^2\right\}\right]^{\frac{n-1}{2}}$$

$$+2\eta_0\frac{\partial v}{\partial y}\frac{\partial}{\partial y}\left[1 + \Gamma^2\left\{4\left(\frac{\partial u}{\partial x}\right)^2 + \left(\frac{\partial u}{\partial y} + \frac{\partial v}{\partial x}\right)^2\right\}\right]^{\frac{n-1}{2}}$$

$$+\eta_0\left(\frac{\partial u}{\partial y} + \frac{\partial v}{\partial x}\right)\frac{\partial}{\partial x}\left[1 + \Gamma^2\left\{4\left(\frac{\partial u}{\partial x}\right)^2 + \left(\frac{\partial u}{\partial y} + \frac{\partial v}{\partial x}\right)^2\right\}\right]^{\frac{n-1}{2}}. \tag{13}$$

We proceed by putting the above equations into non-dimensional form using the standard approach by taking L as typical length and U as stretching speed. The dimensionless variables are defined by

$$(u^*, v^*) = \left(\frac{u}{U}, \frac{v}{U}\right), \quad (x^*, y^*) = \left(\frac{x}{L}, \frac{y}{L}\right), \quad \text{and} \quad p^* = \frac{p}{\rho U^2}. \tag{14}$$

Making use of these non-dimensional variables allows us to write the continuity and momentum transport equations as:

$$\frac{\partial u^*}{\partial x^*} + \frac{\partial v^*}{\partial y^*} = 0, \tag{15}$$

$$u^*\frac{\partial u^*}{\partial x^*} + v^*\frac{\partial u^*}{\partial y^*} = -\frac{1}{\rho}\frac{\partial p^*}{\partial x^*} + \varepsilon_1\left(\frac{\partial^2 u^*}{\partial x^{*2}} + \frac{\partial^2 u^*}{\partial y^{*2}}\right)\left[1 + \varepsilon_2\left\{4\left(\frac{\partial u^*}{\partial x^*}\right)^2 + \left(\frac{\partial u^*}{\partial y^*} + \frac{\partial v^*}{\partial x^*}\right)^2\right\}\right]^{\frac{n-1}{2}}$$

$$+2\varepsilon_1\frac{\partial u^*}{\partial x^*}\frac{\partial}{\partial x^*}\left[1 + \varepsilon_2\left\{4\left(\frac{\partial u^*}{\partial x^*}\right)^2 + \left(\frac{\partial u^*}{\partial y^*} + \frac{\partial v^*}{\partial x^*}\right)^2\right\}\right]^{\frac{n-1}{2}}$$

$$+\varepsilon_1(\frac{\partial u^*}{\partial y^*} + \frac{\partial v^*}{\partial x^*})\frac{\partial}{\partial y^*}\left[1 + \varepsilon_2\left\{4\left(\frac{\partial u^*}{\partial x^*}\right)^2 + \left(\frac{\partial u^*}{\partial y^*} + \frac{\partial v}{\partial x^*}\right)^2\right\}\right]^{\frac{n-1}{2}}, \tag{16}$$

$$u^*\frac{\partial v^*}{\partial x^*} + v^*\frac{\partial v^*}{\partial y^*} = -\frac{1}{\rho}\frac{\partial p^*}{\partial y^*} + \varepsilon_1\left(\frac{\partial^2 v^*}{\partial x^2} + \frac{\partial^2 v^*}{\partial y^{*2}}\right)\left[1 + \varepsilon_2\left\{4\left(\frac{\partial u^*}{\partial x^*}\right)^2 + \left(\frac{\partial u^*}{\partial y^*} + \frac{\partial v^*}{\partial x^*}\right)^2\right\}\right]^{\frac{n-1}{2}}$$

$$+2\varepsilon_1\frac{\partial v^*}{\partial y^*}\frac{\partial}{\partial y^*}\left[1 + \varepsilon_2\left\{4\left(\frac{\partial u^*}{\partial x^*}\right)^2 + \left(\frac{\partial u^*}{\partial y^*} + \frac{\partial v^*}{\partial x^*}\right)^2\right\}\right]^{\frac{n-1}{2}}$$

$$+\varepsilon_1\left(\frac{\partial u^*}{\partial y^*} + \frac{\partial v^*}{\partial x^*}\right)\frac{\partial}{\partial x^*}\left[1 + \varepsilon_2\left\{4\left(\frac{\partial u^*}{\partial x^*}\right)^2 + \left(\frac{\partial u^*}{\partial y^*} + \frac{\partial v^*}{\partial x^*}\right)^2\right\}\right]^{\frac{n-1}{2}}, \tag{17}$$

where the dimensionless parameters ε_1 and ε_2 are defined by

$$\varepsilon_1 = \frac{\eta_0/\rho}{LU} \quad \text{and} \quad \varepsilon_2 = \frac{\Gamma^2}{(L/U)^2}. \tag{18}$$

As we know that in the usual boundary layer approximations, the order of x and u is taken to be 1 while the order of v and y is δ. Furthermore, the dimensionless parameter ε_1 and ε_2 have the order δ^2.

Consequently, using the boundary layer analysis, the above equations in the dimensional form result in

$$\frac{\partial u}{\partial x} + \frac{\partial v}{\partial y} = 0, \tag{19}$$

$$u\frac{\partial u}{\partial x} + v\frac{\partial u}{\partial y} = -\frac{1}{\rho}\frac{\partial p}{\partial x} + v\frac{\partial^2 u}{\partial y^2}\left[1 + \Gamma^2\left(\frac{\partial u}{\partial y}\right)^2\right]^{\frac{n-1}{2}} + v\frac{\partial u}{\partial y}\frac{\partial}{\partial y}\left[1 + \Gamma^2\left(\frac{\partial u}{\partial y}\right)^2\right]^{\frac{n-1}{2}}, \tag{20}$$

$$0 = -\frac{1}{\rho}\frac{\partial p}{\partial y}, \tag{21}$$

where $v = \frac{\eta_0}{\rho}$ is the kinematic viscosity.

The governing equation (20) can also be written in the form

$$u\frac{\partial u}{\partial x} + v\frac{\partial u}{\partial y} = -\frac{1}{\rho}\frac{\partial p}{\partial x} + \nu\frac{\partial^2 u}{\partial y^2}\left[1 + \Gamma^2\left(\frac{\partial u}{\partial y}\right)^2\right]^{\frac{n-1}{2}} + \nu(n-1)\Gamma^2\frac{\partial^2 u}{\partial y^2}\left(\frac{\partial u}{\partial y}\right)^2\left[1 + \Gamma^2\left(\frac{\partial u}{\partial y}\right)^2\right]^{\frac{n-3}{2}}.$$

(22)

III. PROBLEM FORMULATION

We consider the problem of an incompressible two-dimensional flow of a generalized non-Newtonian fluid, namely Carreau fluid, due to a stretching sheet which coincides with the plane $y = 0$. It is assumed that the flow being confined to $y > 0$. The stretching sheet has uniform temperature T_w with T_∞ $(T_w > T_\infty)$ as the ambient fluid temperature and it is moving with a non-linear velocity $U_w = bx^m$. The parameters b and $m(> 0)$ are positive real numbers relating to the stretching speed. The x − coordinate is taken along the moving surface and the y − coordinate is taken normal to it.

Keeping the above assumptions in mind, the governing equations of the problems are

$$\frac{\partial u}{\partial x} + \frac{\partial v}{\partial y} = 0,$$

(23)

$$u\frac{\partial u}{\partial x} + v\frac{\partial u}{\partial y} = \nu\frac{\partial^2 u}{\partial y^2}\left[1 + \Gamma^2\left(\frac{\partial u}{\partial y}\right)^2\right]^{\frac{n-1}{2}} + \nu(n-1)\Gamma^2\frac{\partial^2 u}{\partial y^2}\left(\frac{\partial u}{\partial y}\right)^2\left[1 + \Gamma^2\left(\frac{\partial u}{\partial y}\right)^2\right]^{\frac{n-3}{2}},$$

(24)

$$u\frac{\partial T}{\partial x} + v\frac{\partial T}{\partial y} = \alpha\frac{\partial^2 T}{\partial y^2},$$

(25)

where $\alpha = \frac{k}{\rho c_p}$, c_p is the specific heat and k being the thermal conductivity.

The associated boundary conditions are:

$$u = U_w(x) = bx^m, \quad v = 0, \quad T = T_w \quad at \quad \eta = 0,$$

(26)

$$u \to 0, \quad T \to T_\infty \quad as \quad \eta \to \infty.$$

(27)

The governing momentum and heat transfer equations can be transferred into the coupled ordinary differential equations by introducing the following suitable transformations:

$$\psi(x, y) = \sqrt{\frac{2\nu b}{m+1}}x^{\frac{m+1}{2}}f(\eta), \quad \theta(\eta) = \frac{T - T_\infty}{T_w - T_\infty} \quad \eta = y\sqrt{\frac{b(m+1)}{2\nu}}x^{\frac{m-1}{2}}.$$

(28)

where ψ is the stream function.

TABLE I. A Comparison of the values of $-f''(0)$ with $n = 1.0$, $We = 0.0$, for different values of m.

m	Cortell[19]	Cortell[22]	Hamad and Ferdows[23]	Present study
0.0	-	0.627547	0.6369	0.6275549
0.1	0.705897	-		0.7059245
0.2	-	0.766758	0.7659	0.766837
0.3	0.815696	-		0.815713
0.5	-	0.889477	0.8897	0.889544
0.6	0.918172	-		0.918177
0.75	-	0.953786		0.953957
0.9	0.983242	-		0.983247
1.0	1.0	1.0	1.0043	1.0
1.5	1.061587	1.061587		1.061601
3.0	1.148588	1.148588	1.1481	1.148593
7.0	-	1.216847		1.216851
10.0	1.234875	1.234875	1.2342	1.234875
20.0	-	1.257418	1.2574	1.257424

TABLE II. A Comparison of the values of $-\theta'(0)$ with $n = 1.0$, $We = 0.0$, and $Pr = 1.0$, for different values of m.

m	Cortell[22] with Pr = 1.0	Present study with Pr = 1.0	Cortell[22] with Pr = 1.0	Present study with Pr = 1.0
0.2	0.610262	0.610202	1.607175	1.607130
0.5	0.595277	0.595201	1.586744	1.586759
1.5	0.574537	0.574730	1.557463	1.557519
3.0	0.564472	0.564662	1.542337	1.542719
10.0	0.554960	0.554951	1.528573	1.528502

TABLE III. Numerical values of the local skin friction coefficients $-Re^{\frac{1}{2}}C_{f_x}$ for various values of n, We, and m.

Parameters (fixed values)	Parameters		$-Re^{\frac{1}{2}}C_{f_x}$
$m = 1.0, We = 3.0,$	n	0.5	0.749994
		1.0	1.0
		1.5	1.19396
		2.0	1.35565
		2.5	1.49594
$n = 0.5, We = 3.0$	m	1.0	0.749994
		2.0	0.988647
		3.0	1.17864
		4.0	1.34149
		5.0	1.48641
$n = 0.5, m = 1.0$	We	0.5	0.982634
		1.0	0.938202
		2.0	0.832767
		4.0	0.689758
		5.0	0.644164

TABLE IV. Numerical values of the local Nusselt number $-Re^{-1/2}Nu_x$ for various values of n, We, Pr and m.

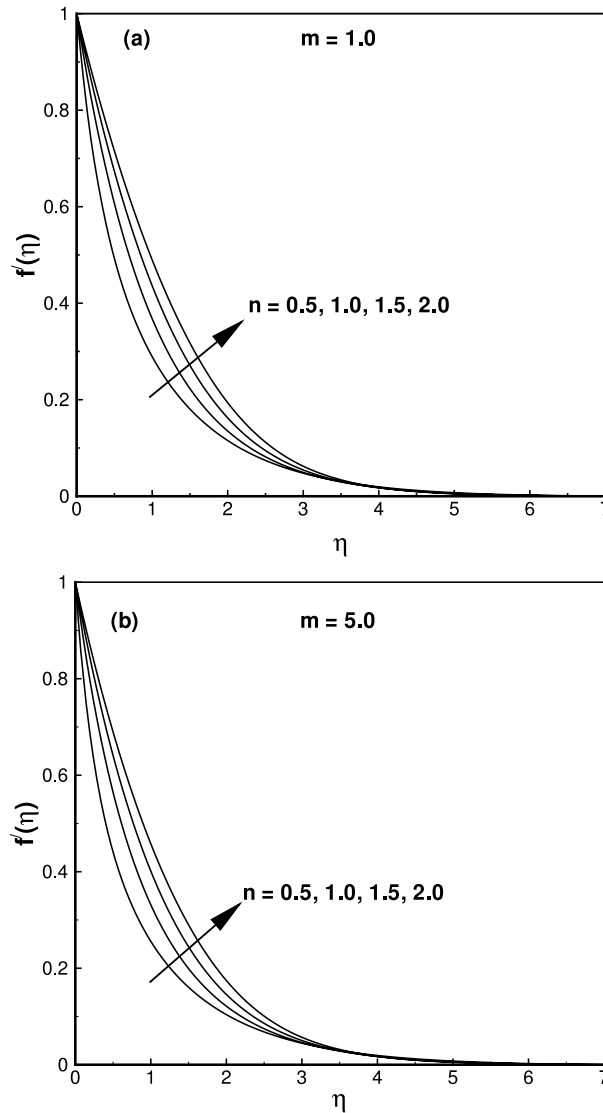| Parameters (fixed values)	Parameters		$-Re^{-1/2}Nu_x$
$m = 1.0, We = 3.0, Pr = 1.0$	n	0.5	0.524684
		1.0	0.582069
		1.5	0.617530
		2.0	0.641585
		2.5	0.658939
$n = 0.5, We = 3.0, Pr = 1.0$	m	1.0	0.524684
		2.0	0.623890
		3.0	0.712031
		4.0	0.789697
		5.0	0.860536
$n = 0.5, m = 1.0, Pr = 1.0$	We	0.5	0.578418
		1.0	0.569132
		2.0	0.545317
		4.0	0.508464
		5.0	0.496211
$n = 0.5, m = 1.0, We = 3.0$	Pr	0.5	0.322215
		1.0	0.524684
		1.5	0.691768
		2.0	0.835148
		2.5	1.078587

FIG. 1. The velocity profile $f'(\eta)$ for several values of the power law index n when $We = 3$ is fixed.

The momentum and energy equations (24) and (25) are thus transformed to:

$$\left\{1 + nWe^2(f'')^2\right\}\left\{1 + We^2(f'')^2\right\}^{\frac{n-3}{2}} f''' + ff'' - \left(\frac{2m}{m+1}\right)(f')^2 = 0, \qquad (29)$$

$$\theta'' + \Pr f\theta' = 0, \qquad (30)$$

where prime denotes differentiation with respect to η, $We = \left(\frac{b^3(m+1)\Gamma^2 x^{3m-1}}{2\nu}\right)^{1/2}$ the local Weissenberg number and $\Pr = \frac{\mu c_p}{k}$ the Prandtl number.

The relevant boundary conditions becomes:

$$f(0) = 0, \quad f'(0) = 1, \quad \theta(0) = 1, \qquad (31)$$

$$f'(\infty) \to 0, \quad \theta(\infty) \to 0. \qquad (32)$$

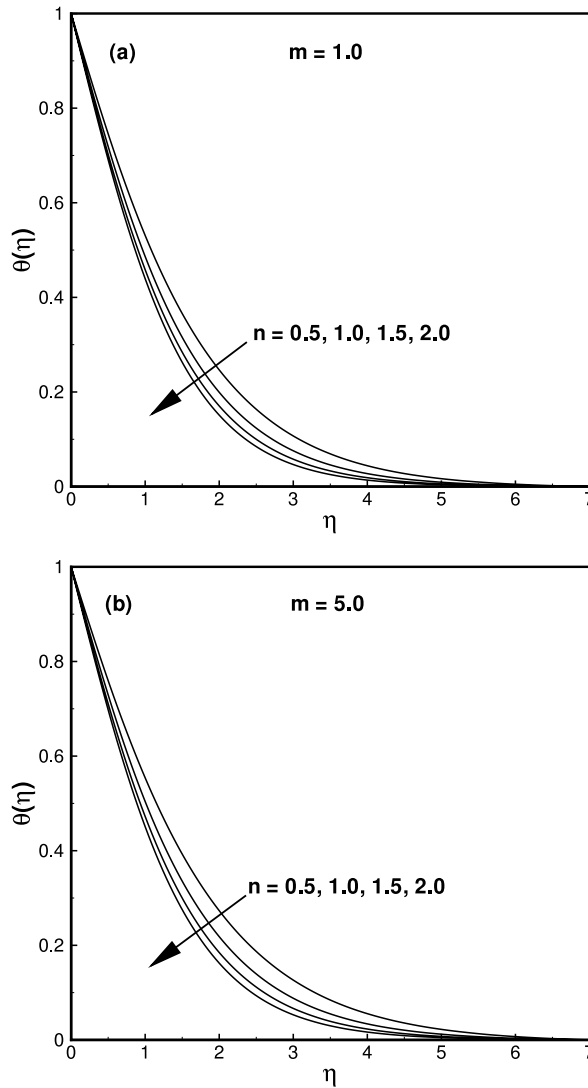It is to be noted that for $n = 1$ or $We = 0$ the Carreau fluid transform to Newtonian fluid.

FIG. 2. The temperature profile $\theta(\eta)$ for several values of the power law index n when $\mathrm{Pr} = 1$ and $We = 3$ are fixed.

The dimensionless physical quantities of practical concern are the local skin friction coefficient C_{f_x} and the local Nusselt number Nu_x, which are given by

$$C_{f_x} = \frac{\tau_w \mid_{y=0}}{\rho U_w^2(x)}, \quad Nu_x = -\frac{x}{(T_w - T_\infty)} \left(\frac{\partial T}{\partial y}\right) \mid_{y=0}, \tag{33}$$

where

$$\tau_w = \eta_0 \frac{\partial u}{\partial y} \left[1 + \Gamma^2\left(\frac{\partial u}{\partial y}\right)^2\right]^{\frac{n-1}{2}}. \tag{34}$$

Thus, using Eq. (34), we obtain

$$\mathrm{Re}^{1/2} C_{f_x} = \sqrt{\frac{m+1}{2}} f''(0)\left[1 + We^2(f''(0))^2\right]^{\frac{n-1}{2}}, \quad \mathrm{Re}^{-1/2} Nu_x = -\sqrt{\frac{m+1}{2}}\theta'(0), \tag{35}$$

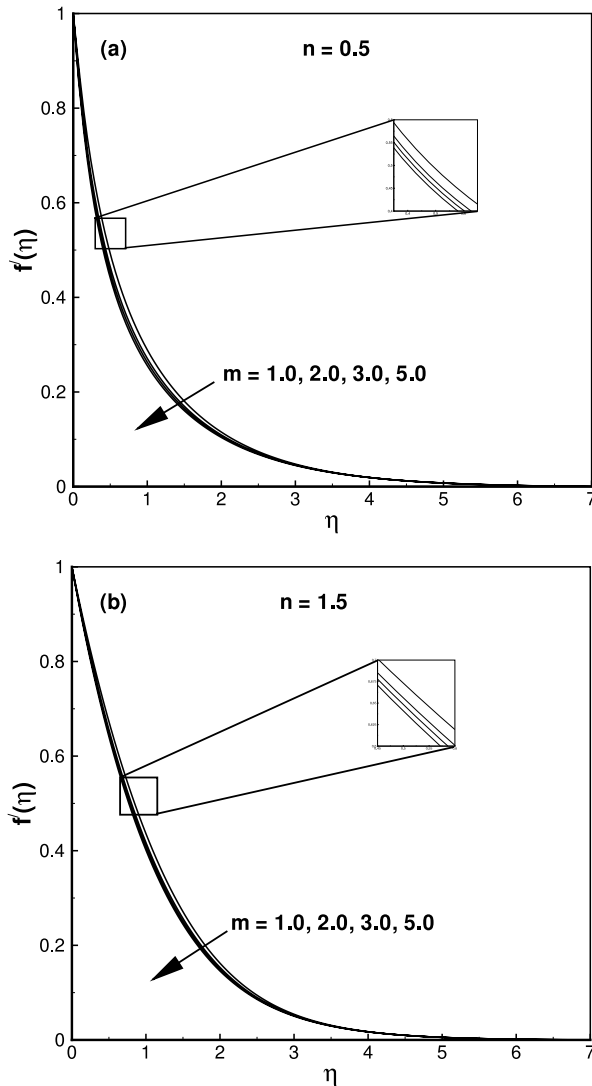where $\mathrm{Re} = \frac{bx^{m+1}}{\upsilon}$ is the local Reynolds number.

FIG. 3. The velocity profile $f'(\eta)$ for several values of the stretching parameter m when $We = 3$ is fixed.

IV. NUMERICAL METHOD FOR SOLUTION

Equations (29) and (30) with associated boundary conditions (31) and (32) are solved using the numerical scheme known as Runge-Kutta Fehlberg method along with shooting technique. In this method we convert the boundary value problem into IVP as:

$$w_1' = w_2, \quad w_2' = w_3, \quad w_3' = \frac{\left[\left(\frac{2m}{m+1}\right)w_2^2 - w_1 w_3\right]}{\left[1 + nWe^2 w_3^2\right]\left[1 + We^2 w_3^2\right]^{\left(\frac{n-3}{2}\right)}}, \tag{36}$$

$$w_4' = w_5, \quad w_5' = -\Pr w_1 w_5, \tag{37}$$

where the prime indicates that the differentiation is carried out with respect to η, $w_1 = f$ and $w_4 = \theta$.

In accordance with the boundary conditions (31) and (32) we have

$$w_1(0) = 0, \quad w_2(0) = 1, \quad w_2(\infty) = 0, \quad w_4(0) = 1, \quad w_4(\infty) = 0. \tag{38}$$

To integrate (36), (37) and (38) as an IVP one requires a value for $w_2(0)$, i.e. $f''(0)$ and $w_4(0)$, i.e. $\theta'(0)$ but no such value is given at the boundary. The initial guess values for $f''(0)$ and $\theta'(0)$ are chosen and then integrated.
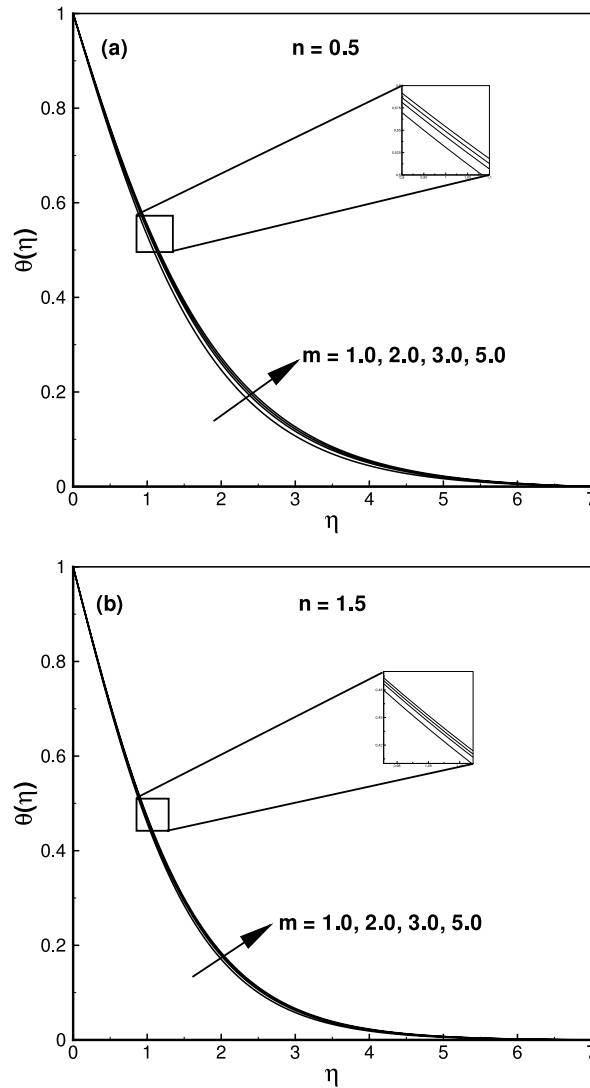
FIG. 4. The temperature profile $\theta(\eta)$ for several values of the stretching parameter m when Pr = 1 and $We = 3$ are fixed.

The main step in shooting scheme is to select the suitable fixed value of η_∞. To estimate η_∞, we start with some initial guess values to pick $f''(0)$ and $\theta'(0)$. We repeat the solution procedure for another large value of η_∞, as far as two consecutive values of $f''(0)$ and $\theta'(0)$ vary only by specific significant digit. The closing value of η_∞ is considered to be the limit of η_∞ for that set of physical quantities. The value of η_∞, may be different for some other set of physical quantities. The obtained values for f' and θ at $\eta = \eta_\infty = 10$ (say) are compared with the corresponding boundary conditions $f'(10) = 0$ and $\theta(10) = 0$. The step-size is taken as $\Delta\eta = 0.01$. We repeat the above procedure until the obtained results converged within a desired tolerance of 10^{-5}.

V. RESULTS AND DISCUSSION

In order to get the physical insight, numerical computations has been performed using the method described in the last section for different values of the Weissenberg number (We), the power law index (n), the stretching parameter (m) and the Prandtl number (Pr). For illustration of these results, numerical solutions are plotted through tables I to IV and figures 1–7.
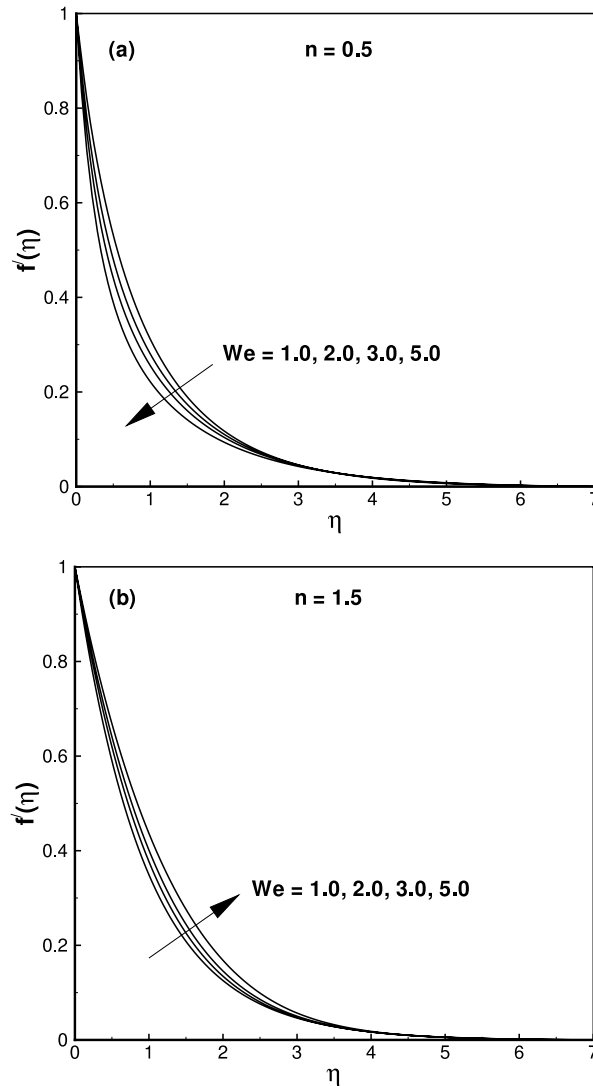
FIG. 5. The velocity profile $f'(\eta)$ for several values of the Weissenberg number We when $m = 5$ is fixed.

In order to check the accuracy of the present results, we have compared our calculated results with those of Cortell,[23] Cortell[26] and Hamad[27] for the skin friction coefficient $\sqrt{\frac{m+1}{2}} f''(0)[1 + We^2\{f''(0)\}^2]^{(\frac{n-1}{2})}$ and rate of heat transfer $-\sqrt{\frac{m+1}{2}} \theta'(0)$ for the power law exponent ($n = 1$) and in the absence of the Weissenberg number ($We = 0$) in the limiting cases. These comparisons are found to be in excellent agreement as shown in tables I and II. Tables III and IV display the calculated numerical values for the local skin friction coefficient and the local Nusselt number. Table III displays that the magnitude of the skin friction increases as the values of n and stretching parameter m increases. Also we can see from the table that by increasing the values of the Weissenberg number We, the skin friction reduces. It is seen from Table IV that for fixed values of Pr, We and m the local Nusselt number increases with an increment in the power law index n. Further the local Nusselt number shows an increasing behavior for the increasing values of the stretching parameter m and the Prandtl number Pr. On the other hand, it is also noted from this table that the local Nusselt number decreases with increase in the Weissenberg number We.

In figures 1 and 2, the physical behavior of the boundary layer near to the surface can be seen by observing the velocity and temperature profiles respectively. These figures demonstrate how
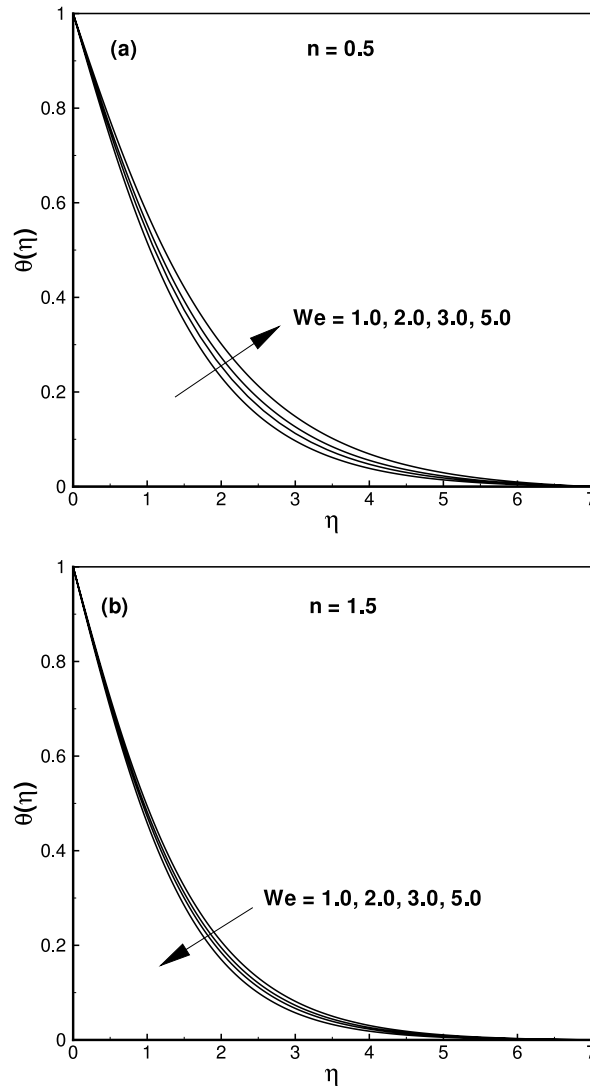
FIG. 6. The temperature profile $\theta(\eta)$ for several values of the Weissenberg number We when $m = 5$ and $Pr = 1$ are fixed.

the velocity and temperature profiles are effected by the power law index n for both linear and non-linear stretching's. The velocity profile $f'(\eta)$ (figure 1) represents an increasing behavior for increasing values of n and temperature profile $\theta(\eta)$ (figure 2) is strongly depressed with increasing power law index n. Further these figures reveal that there is a corresponding increase in the momentum boundary layer thickness while the thermal boundary layer thickness decreases by increasing the power law index n.

Figures 3 and 4 depict the velocity and temperature profiles for distinct values of the stretching parameter m, with varying n. Figure 3 indicates that fluid velocity decreases with the increasing values of the m for both shear thickening ($n > 1$) and shear thinning ($0 < n < 1$) fluids. It is seen that the large values of the stretching parameter m thins the momentum boundary layer thickness. From figure 4, it is evident that the influence of the stretching parameter m is to increase the temperature with its increase and the effects of stretching parameter are more prominent for shear thinning fluid.

Figures 5 and 6 are plotted to illustrate the effects of the Weissenberg number We on the velocity and temperature graphs. Figure 5 examines that the fluid velocity $f'(\eta)$ decreases by uplifting the Weissenberg number for the shear thinning fluid. On the other hand for shear thickening fluid
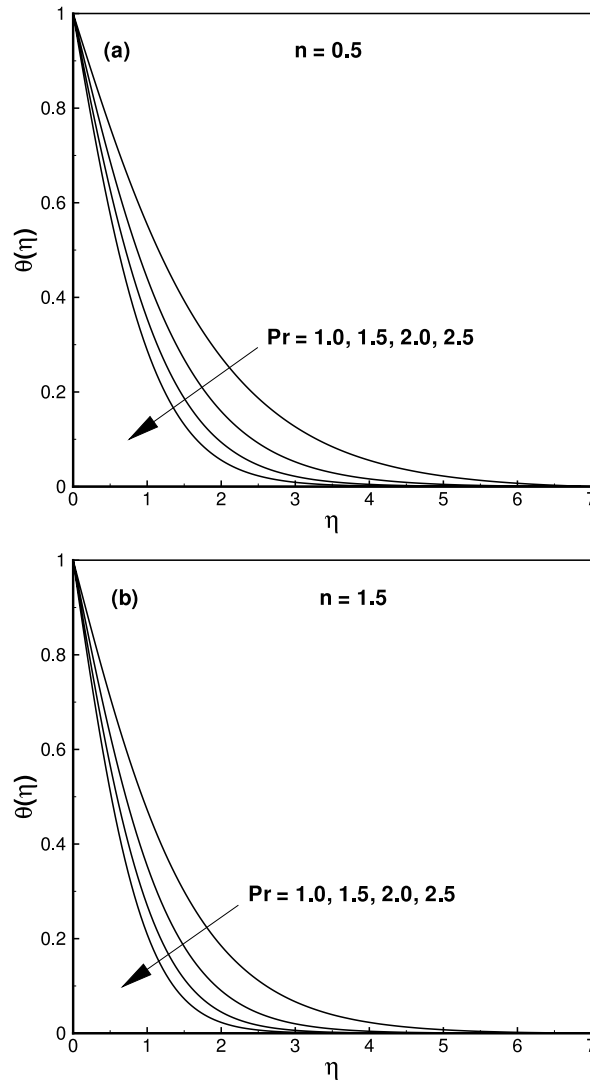
FIG. 7. The temperature profile $\theta(\eta)$ for several values of the Prandtl number Pr when $m = 5$ and $We = 3$ are fixed.

the velocity profile $f'(\eta)$ increases. Influence of the Weissenberg number on the temperature distribution $\theta(\eta)$ is presented in figure 6 and it is clear that the temperature distribution $\theta(\eta)$ increases by increasing the Weissenberg number for the case of shear thinning fluid. While it shows the opposite behavior for the shear thickening fluid.

To see the variation of the Prandtl number on $\theta(\eta)$, figure 7 is plotted for varying values of n. From these figures we can observe that the dimensionless temperature $\theta(\eta)$ reduces with uplifting the Prandtl number Pr and the corresponding thermal boundary layer thickness also decreases for both shear thinning and shear thickening fluids. Physically this is because of the fact that an inflation in the Pr is responsible for the rise in fluid viscosity, which reduces fluid temperature. Furthermore, we see that the thermal boundary layer thickness of the shear thinning fluid is larger than the shear thickening fluid.

VI. CONCLUDING REMARKS

In this study we have obtained the boundary layer equations of motion for a two-dimensional flow of an incompressible non-Newtonian Carreau fluid. The equations for the Newtonian case

can be recovered from the derived equations as a limiting cases. The suitable transformation were employed to reduce the non-linear equations into self-similar ordinary differential equations. The Runge-Kutta Fehlberg method along with shooting technique was used to solve the problem. The results were presented graphically and the effects of the various emerging parameters were discussed. The major findings from the present study are as follows:

- An increase in the momentum boundary layer thickness and a decrease in thermal boundary layer thickness was observed for the increasing values of the power law index including shear thinning to shear thickening fluids.
- Role of the increasing values of the stretching parameter was to thin the momentum boundary layer thickness; however, the opposite trend was noted for thermal boundary layer thickness.
- Increasing the Weissenberg number reduces the magnitude of the fluid velocity for shear thinning fluid while it arises for the shear thickening fluid.
- The temperature and thermal boundary layer thickness was depressed by increasing the Prandtl number Pr.
- An increase in Weissenberg number correspond a decrease in the local skin friction coefficient.
- It was observed that the magnitude of the local Nusselt number was decreased by uplifting the Weissenberg number.

[1] R.B. Bird, C.F. Curtiss, R.C. Armstrong, and O. Hassager, *Dynamics of Polymeric Liquids* (Wiley, New York, 1987).

[2] P.J. Carreau, "Rheological equations from molecular network theories," Trans. Soc. Rheol. **116**, 99–127 (1972).

[3] B. Šiška, H. Bendová, and I. MacHač, "Terminal velocity of non-spherical particles falling through a Carreau model Fluid," Chem. Eng. Process **44**(12), 1312–1319 (2005).

[4] Y.H. Hyun, S.T. Lim, H.J. Choi, and M.S. John, "Rheology of Poly(ethylene oxide)/Organoclay Nanocomposites," Macromolecules **34**(23), 8084–8093 (2001).

[5] D. Corradini, J. Chromatogr, and B. Biomed, "Buffer additives other than the surfactant sodium dodecyl sulfate for protein separations by capillary electrophoresis," Sci. Appl. **699**, 221–256 (1997).

[6] C. Heller, "Principles of DNA separation with capillary electrophoresis," Electrophoresis **22**(4), 629–643 (2001).

[7] R.P. Chhabra and P.H.T. Uhlherr, "Creeping motion of spheres through shear-thinning elastic fluids described by the Carreau viscosity equation," Rheo. Acta. **19**, 187–95 (1980).

[8] M.B. Bush and N. Phan-Thein, "Drag force on a sphere in creeping motion through a Carreau model fluid," J. Non-Newtonian Fluid Mech. **16**, 303–313 (1984).

[9] J.P. Hsu and S.J. Yeh, "Drag on two coaxial rigid spheres moving along the axis of a cylinder filled with Carreau fluid," Powder Technology **182**, 56–71 (2008).

[10] J. Uddin, J.O. Marston, and S.T. Thoroddsen, "Squeeze flow of a Carreau fluid during sphere impact," Phys. Fluids **24**, 073104 (2012).

[11] J.N. Shadid and E.R.G. Eckert, "Viscous heating of a cylinder with finite length by a high viscosity fluid in steady longitudinal flow. II. Non-Newtonian Carreau model fluids," Int J. Heat Mass Transf. **35**(27), 39–49 (1992).

[12] M.S. Tshehla, "The flow of Carreau fluid down an incline with a free surface," Int. J. Phys. Sci. **6**, 3896–3910 (2011).

[13] B.I. Olajuwon, "Convective heat and mass transfer in a hydromagnetic Carreau fluid past a vertical porous plated in presence of thermal radiation and thermal diffusion," Therm. Sci. **15**, 241–252 (2011).

[14] P.T. Griffiths, "Flow of a generalized Newtonian fluid due to a rotating disk," J. Non-Newtonian Fluid Mech. **221**, 9–17 (2015).

[15] B.C. Sakiadis, "Boundary layer behavior on continuous solid surfaces," American Instit. Chem. Engineers **7**, 26–28 (1961).

[16] L.J. Crane, "Flow past a stretching plate," Z. Angew. Math. Phy. **21**(4), 645–647 (1970).

[17] P.S. Gupta and A.S. Gupta, "Heat and mass transfer on a stretching sheet with suction or blowing," Canad. J. Chem. Eng. **55**, 744–746 (1977).

[18] N. S. Akbar, S. Nadeem, R. Ul Haq, and Z. H. Khan, "Numerical solutions of Magnetohydrodynamic boundary layer flow of tangent hyperbolic fluid flow towards a stretching sheet with magnetic field," Indian J. Phys. **87**(11), 1121–1124 (2013).

[19] S. Nadeem, Rizwan Ul Haq, and C. Lee, "MHD flow of a Casson fluid over an exponentially shrinking sheet," Scientia Iranica **19**(6), 1550–1553 (2012).

[20] L.E. Erickson, V.G. Fox, and L.T. Fan, "Heat and mass transfer on a moving continuous flat plate with suction or injection," American Instit. Chemi. Engineers **15**, 327–333 (1969).

[21] N. S. Akbar, Z. H. Khan, R. U. Haq, and S. Nadeem, "Dual solutions in MHD stagnation-point flow of Prandtl fluid impinging on shrinking sheet," Appl. Math. Mech. **35**(7), 813–820 (2014).

[22] K. Vajravelu, "Viscous flow over a nonlinearly stretching sheet," Appl. Math. Comput. **124**(3), 281–288 (2001).

[23] R. Cortell, "Effects of viscous dissipation and radiation on the thermal boundary layer over a non-linearly stretching sheet," Phys. Lett. A **372**, 631–636 (2008).

[24] S. Nadeem, Rizwan Ul Haq, N. S. Akbar, and Z.H. Khan, "MHD three-dimensional Casson fluid flow past a porous linearly stretching sheet," Alexandria Eng. J. **52**(4), 577–582 (2013).

[25] V.D. Boger, "Demonstration of upper and lower Newtonian fluid behavior in a pseudoplastic fluid," Nature **265**, 126–127 (1977).

[26] R. Cortell, "Viscous flow and heat transfer over a nonlinearly stretching sheet," Appl. Math. Comput. **184**, 864–873 (2007).

[27] M.A.A. Hamad and M. Ferdows, "Similarity solutions to viscous flow and heat transfer of nanofluid over nonlinearly stretching sheet," Appl. Math. Mech. Eng. **33**(7), 923–930 (2012).